Mathematical modelling of the stability of carbon nanotube-reinforced panels

B. Sobhani Aragh*

Young Researchers and Elite Club, Arak Branch, Islamic Azad University, Arak, Iran

Abstract.   The present paper studies the stability analysis of the continuously graded CNT-Reinforced Composite (CNTRC) panel stiffened by rings and stringers. The Stiffened Panel (SP) subjected to axial and lateral loads is reinforced by agglomerated CNTs smoothly graded through the thickness. A two-parameter Eshelby-Mori-Tanaka (EMT) model is adopted to derive the effective material moduli of the CNTRC. The stability equations of the CNRTC SP are obtained by means of the adjacent equilibrium criterion. Notwithstanding most available literature in which the stiffener effects were smeared out over the respective stiffener spacing, in the present work, the stiffeners are modeled as Euler-Bernoulli beams. The Generalized Differential Quadrature Method (GDQM) is employed to discretize the stability equations. A numerical study is performed to investigate the influences of different types of parameters involved on the critical buckling of the SP reinforced by agglomerated CNTs. The results achieved reveal that continuously distributing of CNTs adjacent to the inner and outer panel's surface results in improving the stiffness of the SP and, as a consequence, inclining the critical buckling load. Furthermore, it has been concluded that the decline rate of buckling load intensity factor owing to the increase of the panel angle is significantly more sensible for the smaller values of panel angle.

Keywords: panel structure; buckling stability; Generalized Differential Quadrature Method (GDQM); polymer matrix; two-parameter Eshelby-Mori-Tanaka (EMT); carbon-nanotubes; third-order shear deformation theory

1. Introduction

Shell structures, in particular panels, are often reinforced by stiffener elements in order to improve the load-carrying capability with a comparatively small additional weight. The most frequently used stiffeners are the circumferential and meridional stiffeners, which are termed rings and stringers, respectively. When a Stiffened Panel (SP) is subjected to thermo-mechanical loads, they might be buckled. Accordingly, it is mainly imperative to investigate the stability of such structures for effective design and cost-optimized structures. In the past years, a great number of the studies have been allocated to the buckling and post-buckling of the stiffened cylindrical shells and panels composed of Functionally Graded Materials (FGMs) (Shen 2016), which are a new generation of advanced composite materials containing two or more constituent phases with gradually variable distribution. Nevertheless, most of the studies have been established based on the classical shell theory, which does not take into account the important effects of shear deformation and rotatory inertia, resulting in significant inaccuracy, particularly for the larger values of shell's thickness. To name a few, Bich *et al.* (2013) studied the nonlinear static and dynamic buckling of imperfect eccentrically stiffened FG thin circular cylindrical shells subjected to axial compression based on classical thin

shell theory. They concluded that stiffeners are capable of enhancing the static and dynamic stability and load-carrying capacity of FG circular cylindrical shells. Based on Kirchhoff-Love hypothesis, the buckling of stiffened thin-walled shells made of FG metal-ceramic subjected to axial compression loads was investigated by Najafizadeh *et al.* (2009). Dung and Hoa (2013) studied the buckling and post-buckling analysis of eccentrically stiffened FG shells under external pressure. Based on the classical shell theory, the equilibrium equations were derived using the smeared stiffeners technique with the geometrical nonlinearity in von Karman sense. Galerkin method was employed to derive closed-form expressions to obtain the critical buckling loads. An analytical solution for the mechanical buckling of truncated conical shells made of FG metal-ceramic, subjected to axial compressive load and external uniform pressure based on First-order Shear Deformation Theory (FSDT) was presented by Dung and Chan (2017). In this work, the closed-form expression for determining the critical buckling load of the shell was derived. Duc and Thang (2014) studied the nonlinear buckling of imperfect eccentrically stiffened FG thin circular cylindrical shells with temperature-dependent properties resting on the elastic foundation in thermal environment. The results demon-strated that the addition of stiffeners increases the mechanical and thermal loading capacity of the FG shell. Motivated by these considerations, the present paper is established based on the Third-order Shear Deformation Theory (TSDT) of Reddy (1984, 2004) with five unknowns to derive the equilibrium and stability equations of the SP.

The exceptional mechanical behavior and outstanding features of Carbon Nano-Tubes (CNTs) (Iijima 1991) have

---

*Corresponding author, Ph.D.,
  E-mail: behnam.sobhaniaragh@durham.ac.uk;
      behnamsobhani@yahoo.com

made them the best candidate as a reinforcing phase in polymer, ceramic or metal matrix composites. In the last years, the vast majority of the research on the CNT-Reinforced Composites (CNTRCs) has been devoted to polymer matrices (Bououdina 2014) while relatively few efforts (Low 2014) have been made in reinforcing ceramic matrices by CNTs. The combination of extraordinary characteristics of CNTs with intrinsic advantages of ceramic materials such as thermal stability, high corrosion resistance, light density and electrical insulation, generates CNT-Ceramic Matrix Composites (CNT-CMCs) with peculiar functional and structural materials. The potential of developing high-performance CNT-CMCs, which are capable of sustaining conditions of high temperature, chemical attack, and wear, is very attractive with applications as diverse as gas turbines, aerospace materials, and automobiles. Up to now, several micromechanics models, such as the Extended Rule of Mixture (ERM) (Shen 2009, Zhu *et al*. 2012) and Eshelby-Mori-Tanaka (EMT) (Odegard *et al*. 2003, Formica *et al*. 2010, Sobhani Aragh *et al*. 2012) have been employed to estimate the effective mechanical properties of the CNTRCs. As far as the former model is concerned, Shen (2009) extended the conventional rule of mixture by introducing CNT efficiency parameters. The efficiency parameters proposed were derived by matching the elastic moduli of CNTRCs estimated by Molecular Dynamics (MD) and the rule of mixture. In the last years, the ERM has been employed in the vast number of works studying the mechanical responses of such nano-composites structures. However, the ERM deals with critical restrictions since it disregards several intrinsic aspects of CNTs scattered within the matrix of nano-composites, such as agglomeration or waviness. On the other hand, the EMT, which was firstly applied and validated to the CNTRCs by Odegard *et al*. (2003), has played a crucial role in predicting the mechanical properties of nano-composites by considering orientation and agglomeration aspects of CNTs. The EMT is predominantly established based on the equivalent elastic inclusion concept of Eshelby (1957) in combination with the idea of the average stress within the matrix phase proposed by Mori and Tanaka (1973). In particular, notable enhancements and adjustments of the EMT approach were carried out by (Shi *et al*. 2004, Formica and Lacarbonara 2017) to contemplate the CNT agglomeration degree, orientation, curviness and length in combination with experimental study. As reported in various Scanning Electron Microscopy (SEM) image (Talò *et al*. 2016), the outstanding aspects of CNTs such as high stiffness, a peculiar aspect ratio, and strong Van der Waals bonds (Gkikas *et al*. 2012) make them to agglomerate in the nano-composite, especially with ceramic matrix, thereby constituting some local regions with higher concentration of CNTs than the average volume fraction in the nano-composite. Taking the CNT agglomeration effects by means of the EMT model, Sobhaniaragh *et al*. (Mehrabadi and Sobhani Aragh 2014, Hedayati and Sobhani Aragh 2012) studied the natural frequencies and static analyses of nano-composite shells reinforced by agglomerated CNTs. In addition, the interested reader shall refer to Sobhaniaragh's Ph.D. Thesis (Sobhaniaragh 2014) to find comprehensive details on both ERM and EMT. What

is more, this approach has been followed by Fantuzzi *et al*. (2016), Kamarian *et al*. (2016), Tornabene *et al*. (2016), and Moradi-Dastjerdi (2016) to study the influences of agglomeration and distribution of CNTs on the vibration behavior of nano-composites using EMT.

As reported in (Meguid and Sun 2004), the CNT volume fraction should not increase beyond a certain limit to maintain the enhanced mechanical properties. In this regard, the fundamental idea of FGMs might be integrated to the computational modeling of CNTRCs to effectively improve the mechanical function of structures reinforced by CNTs. The FGMs make use of specific desirable features of each constituent phases and tailor the distribution of material properties so that the desired responses to given mechanical and thermal loadings are achieved or natural frequencies are modified to a required manner. In recent years, a number of scholars implemented the concept of gradual gradation of spatial CNT volume fraction in the modeling of nano-composites structures to accomplish desired structural response. Among all available studies, a vast number of papers (Sobhani Aragh *et al*. 2012, Mehrabadi and Sobhani Aragh 2014, Hedayati and Sobhani Aragh 2012, Sobhaniaragh 2014, Fantuzzi *et al*. 2016, Kamarian *et al*, 2016, Tornabene *et al*. 2016, Moradi-Dastjerdi 2016, Madani *et al*. 2016, Nguyen *et al*. 2017, Selim *et al*. 2015, Moradi-Dastjerdi and Momeni-Khabisi 2016, Phung-Van *et al*. 2015, 2017a, b, Sobhani Aragh *et al*. 2013) have been allocated to the bending and vibrational analyses of FG-CNTRCs. Furthermore, the buckling and postbuckling behavior of FG-CNTRCs plates can be found in (Lei *et al*. 2013, Tran *et al*. 2016, Zhang *et al*. 2015, Wang *et al*. 2016). Few studies (Sobhani Aragh *et al*. 2013, Lei *et al*. 2013), however, have been devoted to buckling analysis of the FG-CNTRCs shell structures. It should be noted that the shell studied in all literature (Shen 2011, 2012) has not been reinforced by stiffeners. Recently, García-Macías *et al*. (2017) studied the critical buckling analysis of FG-CNTRC cylindrical curved panels under compression and shear forces by finite elements analysis. The CNTs were assumed to be randomly oriented, distributed in the polymer matrix phase. They concluded that CNTs distributed adjacent to the top and bottom of the panel results in higher stiffness values.

According to the author' literature survey, there is no available study on the mechanical buckling of the SP reinforced by agglomerated CNTs. Consequently, in order to fill in this research gap, the present paper is allocated to investigating the mechanical buckling analysis of the continuously graded SP agglomerated by graded CNTs under axial and lateral loads. Being modelled as Euler-Bernoulli beams, two kinds of stiffeners, i.e., exterior and interior, are considered based on the eccentricity of the stiffeners with respect to the mid-surface of the SP. In the present study, to solve the stability equations the Generalized Differential Quadrature Method (GDQM) (Shu 2012) along with the trigonometric expansion is employed.

2. Theoretical formulations

A continuously graded CNRC SP of finite length L, mean radius R using a global cylindrical coordinate system

(α_1, α_2, α_3) is shown in Fig. 1. The SP is stiffened by means of both circular rings and stringers attached to the shell's skin. Note that the $\bar{Z}_r$ and $\bar{Z}_s$ denote the eccentricity of the stiffeners with respect to the mid-surface of the SP. Additionally, the h_r, b_r and h_s, b_s denote the height and width of the ring and stringers, respectively.

2.1 The two-parameter EMT

A two-parameter EMT model is adopted to predict the effective material properties of the CNTRC. Because of the low bending stiffness and strong Van der Waals bonds (Gkikas *et al.* 2012), CNTs scattered in the CNT have a tendency to aggregate in some regions. That is why such regions encompass higher accumulation of CNTs in comparison with average volume fraction in the whole CNTRC. The EMT model is based on the theory of Eshelby for elastic inclusions. Originally, one single inclusion in a semi-infinite elastic, isotropic, and homogeneous medium forms the limiting assumption of the Eshelby theory. The model is extended by Mori-Tanaka method to capture multiple in-homogeneities embedded into a finite domain. The EMT is fundamentally established based on the equivalent elastic inclusion concept of Eshelby (Eshelby 1957) in combination with the idea of the average stress within the matrix phase intorduced by Mori- Tanaka (Mori and Tanaka 1973). The areas with CNTs accumulated are assumed to have spherical shape and contemplated as inclusions, which have different material properties from outside. As a result, CNTs scattered in the matrix are sorted according to their positions, i.e., embedded inside or outside the inclusions, as shown in Fig. 1. Based on two-parameter EMT model, the total volume V_r of the reinforcing phase is separated into two different parts (Shi *et al.* 2004)

$$V_r = V_r^{inc} + V_r^m \tag{1}$$

where V_r^{inc} and V_r^m designate the volume of CNTs embedded in the inclusions (accumulated areas) and volume of nanotubes dispersed in the matrix phase, respectively. Agglomeration of the CNTs in the matrix results in the mechanical properties of the material to degrade compared with a condition with no CNTs agglomerated. This peculiar aspect of the CNTRCs is described qualitatively by introducing the agglomeration parameters, μ and ξ, given as

$$\mu = \frac{V^{inc}}{V}, \qquad \xi = \frac{V_r^{inc}}{V_r} \tag{2}$$

where V^{inc} is the effective volume of the inclusions, and the parameter μ elaborates the volume fraction of inclusions with regard to the total volume V of the material. If parameter μ is equal unity, there is no agglomeration in matrix phase, and by increasing the parameter μ, the agglomeration degree of CNTs drops. On the other hand, the parameter ξ defines the ratio of nanotubes volume embedded in the inclusions to the total volume of the CNTs. It is obvious that all CNTs are accumulated in the inclusions if ξ equals unity. It is worth noting that the following limitation should be satisfied so that the agglomeration of
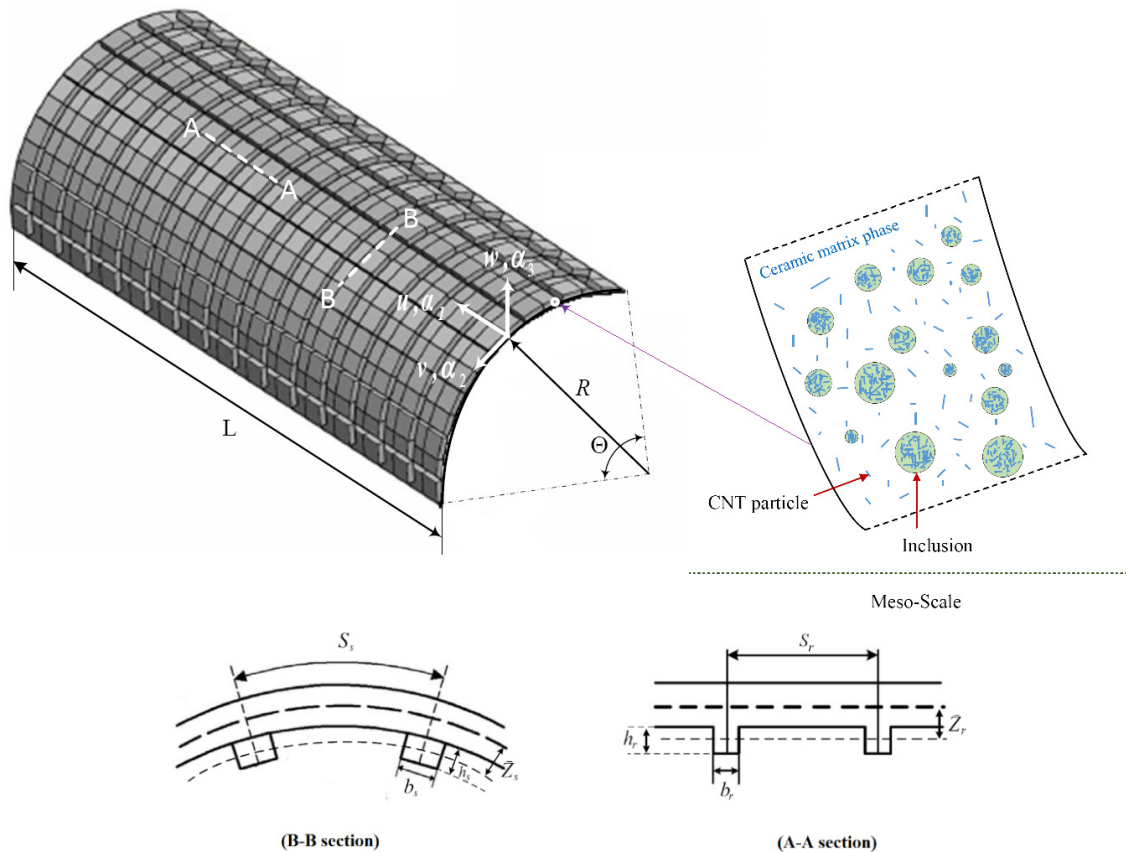

Fig. 1 Schematic plot of the SP aggregated by CNTs

CNTs occurs

$$\xi > \mu \tag{3}$$

To estimate the effective elastic moduli of the inclusions and the matrix phase, it is assumed that the CNTs are transversely isotropic and randomly oriented in the spherical inclusions. The effective bulk modulus $K_{in}(\alpha_3)$ and shear modulus $G_{in}(\alpha_3)$ of the inclusions are expressed by Formica *et al.* (2010) and Shi *et al.* (2004)

$$K_{in}(\alpha_3) = K_m + \frac{f_r(\alpha_3)\xi(\delta_r - 3K_m\alpha_r)}{3(\mu - f_r(\alpha_3)\xi + f_r(\alpha_3)\xi\alpha_r)} \tag{4}$$

$$G_{in}(\alpha_3) = G_m + \frac{f_r(\alpha_3)\xi(\eta_r - 2G_m\beta_r)}{2(\mu - f(\alpha_3)_r\xi + f_r(\alpha_3)\xi\alpha_r)} \tag{5}$$

In a similar manner, the effective bulk modulus $K_{out}(\alpha_3)$ and shear modulus $K_{out}(\alpha_3)$ of the matrix are given

$$K_{out}(\alpha_3) = K_m + \frac{f_r(\alpha_3)(1-\xi)(\delta_r - 3K_m\alpha_r)}{3(1-\mu - f_r(\alpha_3)(1-\xi) + f_r(\alpha_3)(1-\xi)\alpha_r)} \tag{6}$$

$$G_{out}(\alpha_3) = G_m + \frac{f_r(\alpha_3)(1-\xi)(\eta_r - 2G_m\beta_r)}{2(1-\zeta - f_r(\alpha_3)(1-\xi) + f_r(\alpha_3)(1-\xi)\beta_r)} \tag{7}$$

where K_m and G_m denote the bulk and shear moduli of the matrix, respectively, and α_r, β_r, δ_r, and η_r are defined by

$$\alpha_r = \frac{3(K_m + G_m) + k_r + l_r}{3(G_m + k_r)} \tag{8}$$

$$\beta_r = \frac{1}{5}\left[\frac{4G_m + 2k_r + l_r}{3(G_m + k_r)} + \frac{4G_m}{G_m + p_r} \right. \\ \left. + \frac{2[G_m(3K_m + G_m) + G_m(3K_m + 7G_m)]}{G_m(3K_m + G_m) + m_r(3K_m + 7G_m)}\right] \tag{9}$$

$$\delta_r = \frac{1}{3}\left[n_r + 2l_r + \frac{(2k_r + l_r)(3K_m + 2G_m - l_r)}{G_m + k_r}\right] \tag{10}$$

$$\eta_r = \frac{1}{5}\left[\frac{2}{3}(n_r - l_r) + \frac{8G_m p_r}{G_m + p_r} + \frac{2(k_r - l_r)(2G_m + l_r)}{3(G_m + k_r)} \right. \\ \left. + \frac{8m_r G_m(3K_m + 4G_m)}{3K_m(m_r + G_m) + G_m(7m_r + G_m)}\right] \tag{11}$$

in which k_r, m_r, n_r and l_r are the Hill's elastic moduli for the CNTs phase (Cristescu *et al.* 2003, Hill 1965). The relation between the Hill's elastic moduli and material properties of CNTs can be found in Ref. (Tornabene *et al.* 2016). Eventually, the effective bulk modulus $K(\alpha_3)$ and the effective shear modulus $G(\alpha_3)$ of the CNTRC are determined as

$$K(\alpha_3) = K_{out}(\alpha_3)\left[1 + \frac{\mu\left(\dfrac{K_m}{K_{out}(\alpha_3)} - 1\right)}{1 + d^0(\alpha_3)(1-\mu)\left(\dfrac{K_m}{K_{out}(\alpha_3)} - 1\right)}\right] \tag{12}$$

$$G(\alpha_3) = G_{out}(\alpha_3)\left[1 + \frac{\mu\left(\dfrac{G_m}{G_{out}(\alpha_3)} - 1\right)}{1 + \beta(z)(1-\mu)\left(\dfrac{G_m}{G_{out}(\alpha_3)} - 1\right)}\right] \tag{13}$$

in which $v_{out}(z)$ designates the Poisson's ratio of the matrix phase given by

$$v_{out}(\alpha_3) = \frac{3K_{out}(\alpha_3) - 2G_{out}(\alpha_3)}{2[3K_{out}(\alpha_3) + G_{out}(\alpha_3)]} \tag{14}$$

where

$$d^0(\alpha_3) = \frac{1 + v_{out}(\alpha_3)}{3(1 - v_{out}(\alpha_3))} \tag{15}$$

$$\beta(\alpha_3) = \frac{2(4 - 5v_{out}(\alpha_3))}{3(1 - v_{out}(\alpha_3))} \tag{16}$$

Since the CNTRC turns out to be isotropic (Shi *et al.* 2004), the effective Young's modulus $E(\alpha_3)$ and Poisson's ratio $v(\alpha_3)$ of the nano-composite are denoted by

$$E(\alpha_3) = \frac{9K(\alpha_3)G(\alpha_3)}{3K(\alpha_3) + G(\alpha_3)} \tag{17}$$

$$v(\alpha_3) = \frac{3K(\alpha_3) - 2G(\alpha_3)}{6K(\alpha_3) + 2G(\alpha_3)} \tag{18}$$

In the aforementioned relations, $f_r(\alpha_3)$ and $f_m(\alpha_3)$ are the volume fraction of the reinforcing phase and the matrix, which satisfy the relation of $f_r(\alpha_3) + f_m(\alpha_3) = 1$. The volume fraction of CNTs $f_r(\alpha_3)$ is characterized by a smooth variation from the inner to the outer surface of the shell assuming that $f_r(\alpha_3) = V^*_{CNT}V_{CNT}(\alpha_3)$, where V^*_{CNT} is the volume fraction of CNTs (Fidelus *et al.* 2005) and depends on the mass fraction of nanotubes, w_{CNT}, and density of both CNT ρ_{CNT} and the matrix ρ_m

$$V^*_{CNT} = \left[\frac{\rho_{CNT}}{w_{CNT}\rho_m} - \frac{\rho_{CNT}}{\rho_m} + 1\right]^{-1} \tag{19}$$

while $V_{CNT}(z)$ denotes the CNT distribution through the shell's thickness. In this study, it is proposed that the CNT volume fraction follows sigmoidal power-law distribution

$$V_{CNT}(\alpha_3) = \frac{e^{s((\alpha_3/h)+0.5)} - 1}{\left(e^{s/2} - 1\right)\left(e^{s(\alpha_3/h)} + 1\right)} \tag{20}$$
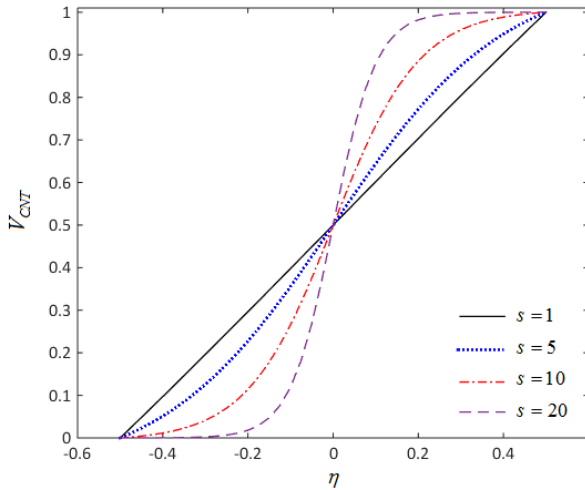
Fig. 2 Through-the-thickness sigmoidal distribution of CNT volume fraction for various sigmoid exponents

in which the sigmoid exponent s controlling the CNT variation profile through the radial direction. This profile demonstrates the sigmoidal variation for various values of sigmoid exponent, as depicted in Fig. 2. The CNT volume fraction presents a linear variation from 0 to 1 in radial direction if $s = 1$. As the sigmoid exponent s increases, the continuously graded panel turns to be a laminated panel with two laminas, whose CNT volume fraction of inner and out surfaces are 0 and V_{CNT}^*, respectively. In the present study, the widely used CNT profiles in the available studies (Shen 2011, 2012, García-Macías *et al.* 2017, Shu 2012), i.e., Profile-X and Profile-O also take into account. As reported in (Sobhani Aragh *et al.* 2012), CNT volume fractions with symmetric distributions through the thickness of the structure have higher capabilities to reduce/increase the natural frequency than those of uniformly and asymmetric distributions.

2.3 Fundamental equations

Based on the TSDT of Reddy (1984, 2004), the displacement components of the mid-surface of the panel along the α_1, α_2 and α_3 axes, denoted by u, v, and w may be expressed as

$$u(\alpha_1,\alpha_2,\alpha_3) = u_0(\alpha_1,\alpha_2) + \alpha_3\psi(\alpha_1,\alpha_2) - C_1\alpha_3^3(\psi + w_{0,\alpha_1})$$

$$v(\alpha_1,\alpha_2,\alpha_3) = v_0(\alpha_1,\alpha_2) + \alpha_3\phi(\alpha_1,\alpha_2) - C_1\alpha_3^3(\phi + w_{0,\alpha_2}) \quad (21)$$

$$w(\alpha_1,\alpha_2,\alpha_3) = w_0(\alpha_1,\alpha_2)$$

in which $C_1 = -4/3h^2$. The nonlinear strain-displacement expression are expressed by

$$\begin{aligned}
\varepsilon_{\alpha_1\alpha_1} &= \varepsilon_{\alpha_1\alpha_1}^{(0)} + \alpha_3\varepsilon_{\alpha_1\alpha_1}^{(1)} + \alpha_3^3\varepsilon_{\alpha_1\alpha_1}^{(3)} \\
\varepsilon_{\alpha_2\alpha_2} &= \varepsilon_{\alpha_2\alpha_2}^{(0)} + \alpha_3\varepsilon_{\alpha_2\alpha_2}^{(1)} + \alpha_3^3\varepsilon_{\alpha_2\alpha_2}^{(3)} \\
\gamma_{\alpha_1\alpha_2} &= \gamma_{\alpha_1\alpha_2}^{(0)} + \alpha_3\gamma_{\alpha_1\alpha_2}^{(1)} + \alpha_3^3\gamma_{\alpha_1\alpha_2}^{(3)} \\
\gamma_{\alpha_1\alpha_3} &= \gamma_{\alpha_1\alpha_3}^{(0)} + \alpha_3^2\gamma_{\alpha_1\alpha_3}^{(2)}
\end{aligned} \quad (22)$$

$$\gamma_{\alpha_2\alpha_3} = \gamma_{\alpha_2\alpha_3}^{(0)} + \alpha_3^2\gamma_{\alpha_2\alpha_3}^{(2)} \quad (22)$$

where

$$\varepsilon_{\alpha_1\alpha_1}^{(0)} = u_{0,\alpha_1} + w_{0,\alpha_1}^2/2 ,$$

$$\varepsilon_{\alpha_2\alpha_2}^{(0)} = v_{0,\alpha_2} + w/R + w_{0,\alpha_2}^2/2$$

$$\gamma_{\alpha_1\alpha_2}^{(0)} = u_{0,\alpha_2} + v_{0,\alpha_1} + w_{0,\alpha_1}w_{0,\alpha_2} ,$$

$$\varepsilon_{\alpha_1\alpha_1}^{(1)} = \psi_{,\alpha_1}$$

$$\varepsilon_{\alpha_2\alpha_2}^{(1)} = \phi_{,\alpha_2} ,$$

$$\gamma_{\alpha_1\alpha_2}^{(1)} = \psi_{,\alpha_2} + \phi_{,\alpha_1} ,$$

$$\varepsilon_{\alpha_1\alpha_1}^{(3)} = -C_1\left(\psi_{,\alpha_1} + w_{0,\alpha_1\alpha_1}\right)$$

$$\varepsilon_{\alpha_2\alpha_2}^{(3)} = -C_1\left(\phi_{,\alpha_2} + w_{0,\alpha_2\alpha_2}\right) , \quad (23)$$

$$\gamma_{\alpha_1\alpha_2}^{(3)} = -C_1\left(\psi_{,\alpha_2} + \phi_{,\alpha_1} + 2w_{0,\alpha_1\alpha_2}\right)$$

$$\gamma_{\alpha_1\alpha_3}^{(0)} = \psi + w_{0,\alpha_1} ,$$

$$\gamma_{\alpha_2\alpha_3}^{(0)} = \phi + w_{0,\alpha_2} ,$$

$$\gamma_{\alpha_1\alpha_3}^{(2)} = -3C_1\left(\psi + w_{0,\alpha_1}\right)$$

$$\gamma_{\alpha_2\alpha_3}^{(2)} = -3C_1\left(\phi + w_{0,\alpha_2}\right)$$

where $\varepsilon_{\alpha_1\alpha_1}$ and $\varepsilon_{\alpha_2\alpha_2}$ denote the normal strains and $\gamma_{\alpha_1\alpha_2}$, $\gamma_{\alpha_1\alpha_3}$ and $\gamma_{\alpha_2\alpha_3}$ are the shear strains. Note that a comma denotes the partial derivative. Based on the 2-D Hooke's law, the constitutive equation of the CNTRC SP is given by

$$\begin{Bmatrix} \sigma_{\alpha_1\alpha_1} \\ \sigma_{\alpha_2\alpha_2} \\ \tau_{\alpha_2\alpha_3} \\ \tau_{\alpha_1\alpha_3} \\ \tau_{\alpha_1\alpha_2} \end{Bmatrix} = \begin{bmatrix} Q_{11} & Q_{12} & 0 & 0 & 0 \\ Q_{21} & Q_{22} & 0 & 0 & 0 \\ 0 & 0 & Q_{44} & 0 & 0 \\ 0 & 0 & 0 & Q_{55} & 0 \\ 0 & 0 & 0 & 0 & Q_{66} \end{bmatrix} \begin{Bmatrix} \varepsilon_{\alpha_1\alpha_1} \\ \varepsilon_{\alpha_2\alpha_2} \\ \gamma_{\alpha_2\alpha_3} \\ \gamma_{\alpha_1\alpha_3} \\ \gamma_{\alpha_1\alpha_2} \end{Bmatrix} \quad (24)$$

in which $[Q]$ is the material stiffness matrix. Notwithstanding most previous works (Bich *et al.* 2013, Najafizadeh *et al.* 2009, Dung and Hoa 2013) in which the stiffener effects were smeared out over the respective stiffener spacing, or in other words, no discrete stiffener effects were treated, in this work, the stiffeners are modeled as Euler-Bernoulli beams, and we assume that prior to bending , the normal vector to the SP and stiffener remains straight after deformation. Consequently, the displacement fields of the Euler-Bernoulli beam are explained as (Reddy 2004).

Ring as a Euler-Bernoulli beam

$$\begin{cases} \overline{u}(\alpha_1,\alpha_2) = v_I(\alpha_1,\alpha_2) - \alpha_3\dfrac{\partial w_I(\alpha_1,\alpha_2)}{\partial \alpha_2} \\ \overline{w}(\alpha_1,\alpha_2) = w_I(\alpha_1,\alpha_2) \end{cases} \quad (25)$$

Sringer as a Euler-Bernoulli beam

$$\begin{cases} \overline{u}(\alpha_1,\alpha_2) = u_I(\alpha_1,\alpha_2) - \alpha_3 \dfrac{\partial w_I(\alpha_1,\alpha_2)}{\partial \alpha_1} \\ \overline{w}(\alpha_1,\alpha_2) = w_I(\alpha_1,\alpha_2) \end{cases} \quad (26)$$

where u_I, v_I, and w_I are the displacements components at I-th nodal location through the SP thickness. The axial, ε_a, and circumferential, ε_c, strains associated with ring and stringer stiffeners are expressed, respectively, by

$$\varepsilon_a = \frac{\partial v_I}{\partial \alpha_2} + \frac{1}{2}(\frac{\partial w_I}{\partial \alpha_2})^2 + \frac{w_I}{R} - \alpha_3(\frac{\partial^2 w_I}{\partial \alpha_2^2}) \quad (27)$$

$$\varepsilon_c = \frac{\partial u_I}{\partial \alpha_1} + \frac{1}{2}(\frac{\partial w_I}{\partial \alpha_1})^2 - \alpha_3(\frac{\partial^2 w_I}{\partial \alpha_1^2}) \quad (28)$$

The Hook's law for rings and stringers is given by

$$\overline{\sigma}_{\alpha_1\alpha_1} = E_s\,\varepsilon_s \quad (29)$$

$$\overline{\sigma}_{\alpha_2\alpha_2} = E_r\,\varepsilon_r \quad (30)$$

where the subscripts "*r*" and "*s*" refer to ring and stringer stiffeners, respectively, and E_i is the Young's modulus. The strain energy of the stringer and ring stiffeners are expressed, respectively, by

$$U_S = \frac{1}{2S_S} \int_0^L \int_0^\Theta \left(\int_{A_S} \sigma_s \varepsilon_s dA + G_S J_S(\frac{\partial^2 w_I}{\partial \alpha_1 \partial \alpha_2}) \right) d\alpha_2 \, d\alpha_1 \quad (31)$$

$$U_r = \frac{1}{2S_r} \int_0^L \int_0^\Theta \left(\int_{A_r} \sigma_r \varepsilon_r dA + G_r J_r(\frac{\partial^2 w_I}{\partial \alpha_1 \partial \alpha_2})^2 \right) d\alpha_2 \, d\alpha_1 \quad (32)$$

Substituting Eqs. (27) and (28) into Eqs. (31) and (32), one obtains

$$U_S = \frac{1}{2S_S} \int_0^L \int_0^\Theta \left[\left(E_s A_s \left(\frac{\partial u_I}{\partial \alpha_1}\right) \right. \right. \\ \left. + \frac{1}{2}\left(\frac{\partial w_I}{\partial \alpha_1}\right)^2 + E_s I_s \left(\frac{\partial^2 w_I}{\partial \alpha_1^2}\right)^2 \right)^2 \\ -2\overline{Z}_s E_s A_s \left(\frac{\partial^2 w_I}{\partial \alpha_1^2}\right)\left(\frac{\partial u_I}{\partial \alpha_1} + \frac{1}{2}\left(\frac{\partial w_I}{\partial \alpha_1}\right)^2\right) \\ \left. + G_s J_s \left(\frac{\partial^2 w_I}{\partial \alpha_1 \partial \alpha_2}\right)^2 \right] d\alpha_2 d\alpha_1 \quad (33)$$

$$U_r = \frac{1}{2S_r} \int_0^L \int_0^\Theta \left[\left(E_r A_r \left(\frac{\partial v_I}{\partial \alpha_2}\right) + \frac{w_I}{R} \right. \right. \\ \left. + \frac{1}{2}\left(\frac{\partial w_I}{\partial \alpha_2}\right)^2 + E_r I_r \left(\frac{\partial^2 w_I}{\partial \alpha_2^2}\right)^2 \right)^2 \\ -2\overline{Z}_r E_r A_r \left(\frac{\partial^2 w_I}{\partial \alpha_2^2}\right)\left(\frac{\partial v_I}{\partial \alpha_2} + \frac{1}{2}\left(\frac{\partial w_I}{\partial \alpha_2}\right)^2 + \frac{w_I}{R}\right) \\ \left. + G_r J_r \left(\frac{\partial^2 w_I}{\partial \alpha_1 \partial \alpha_2}\right)^2 \right] d\alpha_2 d\alpha_1 \quad (34)$$

where

$$\overline{Z}_S = \frac{h+h_s}{2}, \qquad \overline{Z}_r = \frac{h+h_r}{2},$$

$$I_S = \frac{b_s h_s^3}{12} + \overline{Z}_S^2 A_S, \qquad I_r = \frac{b_r h_r^3}{12} + \overline{Z}_r^2 A_r \quad (35)$$

$$J_S = \frac{h_s b_s^3}{3}, \qquad J_r = \frac{h_r b_r^3}{3}$$

in which $S_S = \Theta R/N_s$, $S_r = L/N_r$, N_r, and N_s are the spacing of the ring and stringer stiffeners, respectively. Additionally, the I_r and I_s represent the moment of inertia of the ring and stringer with respect to the mid-surface, respectively. Substituting Eqs. (22) and (24) into the forces and moments relations of the SP (Reddy 2004), we obtain the following expressions for force and moment resultants of the continuously graded CNTRC SP as

$$N_{\alpha_1\alpha_1} = A_{11}\varepsilon_{\alpha_1\alpha_1}^{(0)} + B_{11}\varepsilon_{\alpha_2\alpha_2}^{(0)} + A_{22}\varepsilon_{\alpha_1\alpha_1}^{(1)} + B_{22}\varepsilon_{\alpha_2\alpha_2}^{(1)} + A_{44}\varepsilon_{\alpha_1\alpha_1}^{(3)}$$

$$N_{\alpha_2\alpha_2} = \left(B_{11}\varepsilon_{\alpha_1\alpha_1}^{(0)} + A_{11}\varepsilon_{\alpha_2\alpha_2}^{(0)} \right) \\ + \left(B_{22}\varepsilon_{\alpha_1\alpha_1}^{(1)} + A_{22}\varepsilon_{\alpha_2\alpha_2}^{(0)} \right) + \left(B_{44}\varepsilon_{\alpha_1\alpha_1}^{(3)} + A_{44}\varepsilon_{\alpha_2\alpha_2}^{(3)} \right)$$

$$N_{\alpha_1\alpha_2} = D_{11}\gamma_{\alpha_1\alpha_2}^{(0)} + D_{22}\gamma_{\alpha_1\alpha_2}^{(1)} + D_{44}\gamma_{\alpha_1\alpha_2}^{(3)}$$

$$M_{\alpha_1\alpha_1} = \left(A_{22}\varepsilon_{\alpha_1\alpha_1}^{(0)} + B_{22}\varepsilon_{\alpha_2\alpha_2}^{(0)} \right) \\ + \left(A_{33}\varepsilon_{\alpha_1\alpha_1}^{(1)} + B_{33}\varepsilon_{\alpha_2\alpha_2}^{(1)} \right) + \left(A_{55}\varepsilon_{\alpha_1\alpha_1}^{(3)} + B_{55}\varepsilon_{\alpha_2\alpha_2}^{(3)} \right)$$

$$M_{\alpha_1\alpha_1} = \left(B_{22}\varepsilon_{\alpha_1\alpha_1}^{(0)} + A_{22}\varepsilon_{\alpha_2\alpha_2}^{(0)} \right) \\ + \left(B_{33}\varepsilon_{\alpha_1\alpha_1}^{(1)} + A_{33}\varepsilon_{\alpha_2\alpha_2}^{(0)} \right) + \left(B_{55}\varepsilon_{\alpha_1\alpha_1}^{(3)} + A_{55}\varepsilon_{\alpha_2\alpha_2}^{(3)} \right) \quad (36)$$

$$M_{\alpha_1\alpha_2} = D_{22}\gamma_{\alpha_1\alpha_2}^{(0)} + D_{33}\gamma_{\alpha_1\alpha_2}^{(1)} + D_{55}\gamma_{\alpha_1\alpha_2}^{(3)}$$

$$P_{\alpha_1\alpha_1} = \left(A_{44}\varepsilon_{\alpha_1\alpha_1}^{(0)} + B_{44}\varepsilon_{\alpha_2\alpha_2}^{(0)} \right) \\ + \left(A_{55}\varepsilon_{\alpha_1\alpha_1}^{(1)} + B_{55}\varepsilon_{\alpha_2\alpha_2}^{(1)} \right) + \left(A_{77}\varepsilon_{\alpha_1\alpha_1}^{(3)} + B_{77}\varepsilon_{\alpha_2\alpha_2}^{(3)} \right)$$

$$P_{\alpha_2\alpha_2} = \left(B_{44}\varepsilon_{\alpha_1\alpha_1}^{(0)} + A_{44}\varepsilon_{\alpha_2\alpha_2}^{(0)} \right) \\ + \left(B_{55}\varepsilon_{\alpha_1\alpha_1}^{(1)} + A_{55}\varepsilon_{\alpha_2\alpha_2}^{(0)} \right) + \left(B_{77}\varepsilon_{\alpha_1\alpha_1}^{(3)} + A_{77}\varepsilon_{\alpha_2\alpha_2}^{(3)} \right)$$

$$P_{\alpha_1\alpha_2} = D_{44}\gamma^{(0)}_{\alpha_1\alpha_2} + D_{55}\gamma^{(1)}_{\alpha_1\alpha_2} + D_{77}\gamma^{(3)}_{\alpha_1\alpha_2}$$

$$Q_{\alpha_1\alpha_3} = D_{11}\gamma^{(0)}_{\alpha_1\alpha_3} + D_{33}\gamma^{(2)}_{\alpha_1\alpha_3}$$

$$Q_{\alpha_2\alpha_3} = D_{11}\gamma^{(0)}_{\alpha_2\alpha_3} + D_{33}\gamma^{(2)}_{\alpha_2\alpha_3} \tag{36}$$

$$R_{\alpha_1\alpha_3} = D_{33}\gamma^{(0)}_{\alpha_1\alpha_3} + D_{55}\gamma^{(2)}_{\alpha_1\alpha_3}$$

$$R_{\alpha_2\alpha_3} = D_{33}\gamma^{(0)}_{\alpha_2\alpha_3} + D_{55}\gamma^{(2)}_{\alpha_2\alpha_3}$$

in which

$$\{A_{11}, A_{22}, A_{33}, A_{44}, A_{55}, A_{77}\}$$
$$= \int_{-h/2}^{h/2} Q_{11}(\alpha_3)(1, \alpha_3, \alpha_3^2, \alpha_3^3, \alpha_3^4, \alpha_3^6)d\alpha_3$$
$$\{B_{11}, B_{22}, B_{33}, B_{44}, B_{55}, B_{77}\}$$
$$= \int_{-h/2}^{h/2} Q_{12}(\alpha_3)(1, \alpha_3, \alpha_3^2, \alpha_3^3, \alpha_3^4, \alpha_3^6)d\alpha_3 \tag{37}$$
$$\{D_{11}, D_{22}, D_{33}, D_{44}, D_{55}, D_{77}\}$$
$$= \int_{-h/2}^{h/2} Q_{44}(\alpha_3)(1, \alpha_3, \alpha_3^2, \alpha_3^3, \alpha_3^4, \alpha_3^6)d\alpha_3$$

The equilibrium equations of the continuously graded SP subjected to mechanical loads can be derived on the basis of the stationary potential energy criterion. The total potential energy of a panel stiffened by ring and stringer stiffeners is defined as (Reddy 2004)

$$V = U + \Omega \tag{38}$$

where Ω designate the potential energy of the applied loads, and U is the total strain energy of the SP, which is given by

$$U = U_{Sh} + U_r + U_S \tag{39}$$

where U_{Sh} represents the strain energy of the panel. The total strain energy U_{Sh} for the panel based on the TSDT may be written

$$U_{sh} = \int_0^L\int_0^\Theta\int_{-h/2}^{h/2} (\sigma_{\alpha_1\alpha_1}\varepsilon_{\alpha_1\alpha_1} + \sigma_{\alpha_2\alpha_2}\varepsilon_{\alpha_2\alpha_2} + \tau_{\alpha_1\alpha_2}\gamma_{\alpha_1\alpha_2}$$
$$+ \tau_{\alpha_1\alpha_3}\gamma_{\alpha_1\alpha_3} + \tau_{\alpha_2\alpha_3}\gamma_{\alpha_2\alpha_3})d\alpha_3\,d\alpha_2\,d\alpha_1 \tag{40}$$

The potential energy of the loads, Ω, for a conservative system is defined as the negative of work done by applied loads as the shell is deformed. Consequently, for the lateral pressure, $N_{0\alpha_2}$ and axial compressive edge load, $N_{0\alpha_1}$, it is expressed by Reddy (2004)

$$\Omega = \frac{1}{2}\int_0^L\int_0^\Theta \left(N_{0\alpha_1} + N_{0\alpha_2}\right)\left((w_{,\alpha_1})^2 + (v_{,\alpha_1})^2\right)d\alpha_2 d\alpha_1 \tag{41}$$

It is worth noting that the contribution of the $(v_{,\alpha_1})^2$ term in the buckling of the panel with short or moderate length is negligible. In other words, the shortening owing to circumferential displacement of the panel under mechanical

buckling can be omitted for the panels with length-to-radius ratio between 0.7 and 3 (Lim *et al.* 2003). Substituting Eqs. (33-34), (40-41) into Eq. (39), the total potential energy of the SP is defined by

$$U = R\int_0^L\int_0^\Theta \left\{ \frac{1}{2}\left(A_{11}\varepsilon^{(0)^2}_{\alpha_1\alpha_1} + A_{11}\varepsilon^{(0)^2}_{\alpha_2\alpha_2} \right.\right.$$
$$+ 2B_{11}\varepsilon^{(0)}_{\alpha_1\alpha_1}\varepsilon^{(0)}_{\alpha_2\alpha_2} + D_{11}\left(\gamma^{(0)^2}_{\alpha_1\alpha_2} + \gamma^{(0)^2}_{\alpha_1\alpha_3} + \gamma^{(0)^2}_{\alpha_2\alpha_3}\right) \bigg)$$
$$+ \frac{1}{2}\bigg(A_{22}\varepsilon^{(1)}_{\alpha_1\alpha_1}\varepsilon^{(0)}_{\alpha_1\alpha_1} + A_{22}\varepsilon^{(1)}_{\alpha_2\alpha_2}\varepsilon^{(0)}_{\alpha_2\alpha_2} + B_{22}\varepsilon^{(1)}_{\alpha_2\alpha_2}\varepsilon^{(0)}_{\alpha_1\alpha_1}$$
$$+ B_{22}\varepsilon^{(1)}_{\alpha_1\alpha_1}\varepsilon^{(0)}_{\alpha_2\alpha_2} + D_{22}\left(\gamma^{(0)}_{\alpha_1\alpha_2}\gamma^{(1)}_{\alpha_1\alpha_2}\right) \bigg)$$
$$+ \frac{1}{2}\bigg(A_{33}\varepsilon^{(1)\,2}_{\alpha_1\alpha_1} + A_{33}\varepsilon^{(1)\,2}_{\alpha_2\alpha_2} + 2B_{33}\varepsilon^{(1)}_{\alpha_1\alpha_1}\varepsilon^{(1)}_{yy}$$
$$+ D_{33}\left(\gamma^{(1)\,2}_{\alpha_1\alpha_2}\right) + 2D_{33}(\gamma^{(1)}_{\alpha_2\alpha_3}\gamma^{(0)}_{\alpha_2\alpha_3} + \gamma^{(1)}_{\alpha_1\alpha_3}\gamma^{(0)}_{\alpha_1\alpha_3}) \bigg)$$
$$+ \bigg(A_{44}\varepsilon^{(3)}_{\alpha_1\alpha_1}\varepsilon^{(0)}_{\alpha_1\alpha_1} + A_{44}\varepsilon^{(3)}_{\alpha_2\alpha_2}\varepsilon^{(0)}_{\alpha_2\alpha_2}$$
$$+ B_{44}\varepsilon^{(3)}_{\alpha_2\alpha_2}\varepsilon^{(0)}_{\alpha_1\alpha_1} + B_{44}\varepsilon^{(3)}_{\alpha_1\alpha_1}\varepsilon^{(0)}_{\alpha_2\alpha_2} + D_{44}\left(\gamma^{(3)}_{\alpha_1\alpha_2}\gamma^{(0)}_{\alpha_1\alpha_2}\right) \bigg)$$
$$+ \bigg(A_{55}\varepsilon^{(3)}_{\alpha_1\alpha_1}\varepsilon^{(1)}_{\alpha_1\alpha_1} + A_{55}\varepsilon^{(3)}_{\alpha_2\alpha_2}\varepsilon^{(1)}_{\alpha_2\alpha_2} + B_{55}\varepsilon^{(3)}_{\alpha_2\alpha_2}\varepsilon^{(1)}_{\alpha_1\alpha_1}$$
$$+ B_{55}\varepsilon^{(3)}_{\alpha_1\alpha_1}\varepsilon^{(1)}_{\alpha_2\alpha_2} + D_{55}\left(\gamma^{(3)}_{\alpha_1\alpha_2} + \gamma^{(1)}_{\alpha_1\alpha_2}\right) \tag{42}$$
$$+ \frac{D_{55}}{2}\left(\gamma^{(1)\,2}_{\alpha_2\alpha_3} + \gamma^{(1)\,2}_{\alpha_2\alpha_3}\right) \bigg) + \frac{1}{2}\bigg(A_{77}\varepsilon^{(3)\,2}_{\alpha_1\alpha_1} + A_{77}\varepsilon^{(3)\,2}_{\alpha_2\alpha_2}$$
$$+ 2B_{77}\varepsilon^{(3)}_{\alpha_1\alpha_1}\varepsilon^{(3)}_{\alpha_2\alpha_2} + \frac{D_{77}}{2}\left(\gamma^{(3)\,2}_{\alpha_1\alpha_2}\right) \bigg)$$
$$+ \frac{1}{2S_S}\left[E_s A_s\left(\frac{\partial u_1}{\partial\alpha_1} + \frac{1}{2}\left(\frac{\partial w_I}{\partial\alpha_1}\right)^2\right)^2 + E_s I_s\left(\frac{\partial^2 w_I}{\partial\alpha_1^2}\right)^2 \right.$$
$$- 2\bar{Z}_s A_s E_s\left(\frac{\partial^2 w_I}{\partial\alpha_1^2}\right)\left(\frac{\partial u_I}{\partial\alpha_1} + \frac{1}{2}\left(\frac{\partial w_I}{\partial\alpha_1}\right)^2\right)$$
$$+ G_s J_s\left(\frac{\partial^2 w_I}{\partial\alpha_1\partial\alpha_2}\right)^2 \bigg]$$
$$+ \frac{1}{2S_r}\left[E_r A_r\left(\frac{\partial v_I}{\partial\alpha_2} + \frac{w_I}{R} + \frac{1}{2}\left(\frac{\partial w_I}{\partial\alpha_2}\right)^2\right)^2 + E_r I_r\left(\frac{\partial^2 w_I}{\partial\alpha_2^2}\right)^2 \right.$$
$$- 2\bar{Z}_r E_r A_r\left(\frac{\partial^2 w_I}{\partial\alpha_2^2}\right)\left(\frac{\partial v_I}{\partial\alpha_2} + \frac{w_I}{R} + \frac{1}{2}\left(\frac{\partial w_I}{\partial\alpha_2}\right)^2\right)$$
$$+ G_r J_r\left(\frac{\partial^2 w_I}{\partial\alpha_1\partial\alpha_2}\right)^2 \bigg] \bigg\} d\alpha_2 d\alpha_1$$

The equilibrium equation of continuously graded CNTRC SP can be obtained by means of the variational approach. Using the Euler equations (Brush and Almroth 1975), the general equilibrium equations of the SP based on

TSDT are resulted as

$$
N_{\alpha_1\alpha_1,\alpha_1} + N_{\alpha_1\alpha_2,\alpha_2} + \frac{\partial}{\partial\alpha_1}\left\{ \frac{1}{S_x}\left[E_s A_s \left(\frac{\partial u_I}{\partial\alpha_1} \right.\right.\right.
$$
$$
\left.\left.\left. + \frac{1}{2}\left(\frac{\partial u_I}{\partial\alpha_1}\right)^2 \right) - \bar{Z}_s A_s E_s \left(\frac{\partial w_I}{\partial\alpha_1}\right)^2 = 0 \right.\right.
$$
(43)

$$
N_{\alpha_1\alpha_2,\alpha_1} + N_{\alpha_2\alpha_2,\alpha_2} + \frac{\partial}{\partial\alpha_2}\left\{ \frac{1}{S_r}\left[E_r A_r \left(\frac{\partial v_I}{\partial\alpha_2} \right.\right.\right.
$$
$$
\left.\left.\left. + \frac{w_I}{R} + \frac{1}{2}\left(\frac{\partial w_I}{\partial\alpha_2}\right)^2 \right) - \bar{Z}_r A_r E_r \left(\frac{\partial^2 W_I}{\partial\alpha_2^2}\right) \right] \right\} = 0
$$
(44)

$$
-\frac{1}{R}N_{\alpha_2\alpha_2} - \frac{1}{RS_r}\left[E_r A_r \left(\frac{\partial v_I}{\partial\alpha_2} + \frac{w_I}{R} + \frac{1}{2}\left(\frac{\partial w_I}{\partial\alpha_2}\right)^2 \right) \right.
$$
$$
\left. - \bar{Z}_r A_r E_r \left(\frac{\partial^2 w_I}{\partial\alpha_2^2}\right) \right] + N_{\alpha_1\alpha_1} w_{0,\alpha_1\alpha_1}
$$
$$
+ N_{\alpha_2\alpha_2} w_{0,\alpha_2\alpha_2} + 2N_{\alpha_1\alpha_2} w_{0,\alpha_1\alpha_2}
$$
$$
+ N_{0\alpha_2}\left(\frac{\partial^2 w}{\partial\alpha_2^2}\right) + \frac{1}{S_s}\bar{N}_{\alpha_1\alpha_1}\frac{\partial^2 w_I}{\partial\alpha_1^2} -
$$
$$
+ N_{0\alpha_1}\left(\frac{\partial^2 w}{\partial\alpha_1^2}\right) + \frac{1}{S_r}\bar{N}_{\alpha_2\alpha_2}\frac{\partial^2 w_I}{\partial\alpha_2^2} + Q_{\alpha_1\alpha_3,\alpha_1}
$$
$$
+ Q_{\alpha_2\alpha_3,\alpha_2} - 3C_1\left(R_{\alpha_1\alpha_3,\alpha_1} + R_{\alpha_2\alpha_3,\alpha_2}\right)
$$
$$
+ C_1\left(P_{\alpha_1\alpha_1,\alpha_1\alpha_1} + 2P_{\alpha_1\alpha_2,\alpha_1\alpha_2} + P_{\alpha_2\alpha_2,\alpha_2\alpha_2}\right)
$$
$$
- \frac{\partial^2}{\partial\alpha_1^2}\left[\frac{1}{S_s}\left\{ \left(E_s I_s + \bar{Z}_s E_s A_s C_1\left(\frac{h}{2}\right)^3\right)\left(\frac{\partial^2 w_I}{\partial\alpha_1^2}\right) \right.\right.
$$
$$
\left.\left. - \left(\bar{Z}_s A_s E_s + E_s A_s C_1\left(\frac{h}{2}\right)^3\right)\left(\frac{\partial u_I}{\partial\alpha_1} + \frac{1}{2}\left(\frac{\partial w_I}{\partial\alpha_1}\right)^2\right) \right\} \right]
$$
(45)
$$
- \frac{\partial^2}{\partial\alpha_2^2}\left[\frac{1}{S_r}\left\{ \left(E_r I_r + \bar{Z}_r E_r A_r C_1\left(\frac{h}{2}\right)^3\right)\left(\frac{\partial^2 w_I}{\partial\alpha_2^2}\right) \right.\right.
$$
$$
\left.\left. \left(\bar{Z}_r A_r E_r + E_r A_r C_1\left(\frac{h}{2}\right)^3\right)\left(\frac{\partial v_I}{\partial\alpha_2} + \frac{1}{2}\left(\frac{\partial w_I}{\partial\alpha_2}\right)^2 + \frac{w_I}{R}\right) \right\} \right]
$$
$$
- \frac{\partial^2}{\partial\alpha_1\partial\alpha_2}\left[\frac{1}{S_s}(G_s J_s \frac{\partial^2 w_I}{\partial\alpha_1\partial\alpha_2}) \right.
$$
$$
\left. + \frac{1}{S_r}(G_r J_r \frac{\partial^2 w_I}{\partial\alpha_1\partial\alpha_2}) \right] = 0
$$

$$
-Q_{\alpha_1\alpha_3} + 3C_1 R_{\alpha_1\alpha_3} + M_{\alpha_1\alpha_1,\alpha_1} + M_{\alpha_1\alpha_2,\alpha_2}
$$
$$
- C_1\left(P_{\alpha_1\alpha_1,\alpha_1} + P_{\alpha_1\alpha_2,\alpha_2}\right)
$$
$$
+ \frac{\partial}{\partial\alpha_1}\left[\frac{1}{S_s}\left\{ E_s A_s \left(\frac{h}{2} - C_1\left(\frac{h}{2}\right)^2\right) \right.\right.
$$
(46)

$$
\left(\frac{\partial u_I}{\partial\alpha_1} + \frac{1}{2}\left(\frac{\partial w_I}{\partial\alpha_1}\right)^2\right)
$$
$$
\left.\left. - \bar{Z}_s A_s E_s \left(\frac{h}{2} - c_1\left(\frac{h}{2}\right)^3\right)\left(\frac{\partial^2 w_I}{\partial\alpha_1^2}\right) \right\} \right] = 0
$$
(46)

$$
-Q_{\alpha_2\alpha_3} + 3C_1 R_{\alpha_2\alpha_3} + M_{\alpha_1\alpha_2,\alpha_1} + M_{\alpha_2\alpha_2,\alpha_2}
$$
$$
- C_1\left(P_{\alpha_1\alpha_2,\alpha_1} + P_{\alpha_2\alpha_2,\alpha_2}\right)
$$
$$
+ \frac{\partial}{\partial\alpha_2}\left[\frac{1}{S_r}\left\{ E_r A_r \left(\frac{h}{2} - C_1\left(\frac{h}{2}\right)^3\right) \right.\right.
$$
(47)

$$
\left(\frac{\partial v_I}{\partial\alpha_2} + \frac{w_I}{R} + \frac{1}{2}\left(\frac{\partial w_I}{\partial\alpha_2}\right)^2\right)
$$
$$
\left.\left. - \bar{Z}_r A_r E_r \left(\frac{h}{2} - c_1\left(\frac{h}{2}\right)^3\right)\left(\frac{\partial^2 w_I}{\partial\alpha_2^2}\right) \right\} \right] = 0
$$

in which $\bar{N}_{\alpha_1\alpha_1}$ and $\bar{N}_{\alpha_2\alpha_2}$ are the forces applied to the ring and stringer stiffeners given by

$$
\bar{N}_{\alpha_1\alpha_1} = \int_{A_s} \sigma_{\alpha_1\alpha_1} dA = \int_{h/2}^{h/2+h_s} b_s \sigma_s dA
$$
$$
= E_s A_s \left(\frac{\partial u_I}{\partial\alpha_1} + \frac{1}{2}\left(\frac{\partial w_I}{\partial\alpha_1}\right)^2\right) - \bar{Z}_s A_s E_s \left(\frac{\partial^2 w_I}{\partial\alpha_1^2}\right)
$$
(48)

$$
\bar{N}_{\alpha_2\alpha_2} = \int_{A_s} \sigma_{\alpha_2\alpha_2} dA = \int_{h/2}^{h/2+h_r} b_r \sigma_r dA
$$
$$
= E_r A_r \left(\frac{\partial v_I}{\partial\alpha_2} + \frac{1}{2}\left(\frac{\partial w_I}{\partial\alpha_2}\right)^2 + \frac{w_I}{R}\right) - \bar{Z}_r A_r E_r \left(\frac{\partial^2 w_I}{\partial\alpha_2^2}\right)
$$
(49)

Taking the variational approach into account, the stability equations of continuously graded CNTRC SP is derived. Using Taylor series, the total strain energy of the shell is expanded about the equilibrium state as

$$
\Delta V = \delta V + \frac{1}{2}\delta^2 V + \frac{1}{6}\delta^3 V + ...
$$
(50)

in which the first variation, δV, is correlated to the equilibrium state. The stability condition of the configuration of the SP in the vicinity of the state of the equilibrium shall be determined by the sign of second variation, $\delta^2 V$. Additionally, the $\delta^2 V = 0$ leads to the stability equations of the buckling problem (Brush and Almroth 1975). To proceed with the stability equations of the CNTRC SP, the displacement components are expressed by

$$
u_0 = u_0^0 + u_0^1, \qquad v_0 = v_0^0 + v_0^1, \qquad w_0 = w_0^0 + w_0^1
$$
$$
\psi = \psi^0 + \psi^1, \qquad \phi = \phi^0 + \phi^1
$$
(51)

where u_0^0, v_0^0, w_0^0, ψ^0, and ϕ^0 represent the displacement components of the state of the equilibrium. The displacement fields of the vicinity of the stable equilibrium are expressed by u_0^1, v_0^1, w_0^1, ψ^1, and ϕ^1 with regard to the position of the equilibrium. Consequently, two items denoting the stable equilibrium and the neighboring state form the stress resultants. It is worth noting that the applied load imposing on the configuration is deemed to be the critical buckling load if the $\delta^2 V = 0$ is satisfied. Substituting Eqs. (22) and (24) into Eq. (50) and using Eq. (38) and collecting the second-order terms, one can obtain the second variation of the potential energy, upon which employing the Euler equations, results in the stability equations of the SP reinforced by agglomerated graded CNTs as N

$$N^1_{\alpha_1\alpha_1,\alpha_1} + N^1_{\alpha_1\alpha_2,\alpha_2}$$
$$+\frac{\partial}{\partial\alpha_1}\left[\frac{1}{S_s}\left\{E_s A_s\left(\frac{\partial u_I^1}{\partial\alpha_1}\right) - \bar{Z}_s A_s E_s\left(\frac{\partial^2 w_I^1}{\partial\alpha_1^2}\right)\right\}\right] = 0 \quad (52)$$

$$N^1_{\alpha_1\alpha_2,\alpha_1} + N^1_{\alpha_2\alpha_2,\alpha_2}$$
$$+\frac{\partial}{\partial\alpha_2}\left[\frac{1}{S_r}\left(E_r A_r\left(\frac{\partial v_I^1}{\partial\alpha_2}+\frac{w_I^1}{R}\right) - \bar{Z}_r A_r E_r\left(\frac{\partial^2 w_I^1}{\partial\alpha_2^2}\right)\right)\right] = 0 \quad (53)$$

$$\frac{1}{R}N^1_{\alpha_2\alpha_2} - \frac{1}{RS_r}\left\{E_r A_r\left(\frac{\partial v_I^1}{\partial\alpha_2}+\frac{w_I^1}{R}\right) - \bar{Z}E_r A_r\left(\frac{\partial^2 w_I^1}{\partial\alpha_2^2}\right)\right\}$$
$$+ N_{0\alpha_2} w_{1,\alpha_2\alpha_2} + 2N^0_{\alpha_1\alpha_2} w_{1,\alpha_1\alpha_2} + \frac{1}{S_s}\bar{N}^0_{\alpha_1\alpha_1}\frac{\partial^2 w_I^1}{\partial\alpha_1^2}$$
$$+\frac{1}{S_r}\bar{N}^0_{\alpha_2\alpha_2}\frac{\partial^2 w_I^1}{\partial\alpha_2^2} + N_{0\alpha_2} w_{1,\alpha_2\alpha_2}$$
$$+ Q^1_{\alpha_1\alpha_3} + Q^1_{\alpha_2\alpha_3} - 3C_1(R^1_{\alpha_3\alpha_1,\alpha_1} + R^1_{\alpha_2\alpha_3})$$
$$+ C_1(P^1_{\alpha_1\alpha_1,\alpha_1\alpha_1} + 2P^1_{\alpha_1\alpha_2,\alpha_1\alpha_2} + P^1_{\alpha_2\alpha_2,\alpha_2\alpha_2})$$
$$-\frac{\partial^2}{\partial\alpha_1^2}\left[\frac{1}{S_s}\left\{\left(E_s I_s + \bar{Z}E_s A_s C_1\left(\frac{h}{2}\right)^3\right)\left(\frac{\partial^2 w_I^1}{\partial\alpha_1^2}\right)\right.\right.$$
$$\left.\left. -\left(\bar{Z}E_s A_s + E_s A_s C_1\left(\frac{h}{2}\right)^3\right)\left(\frac{\partial u_I^1}{\partial\alpha_1}\right)\right\}\right]$$
$$-\frac{\partial^2}{\partial\alpha_2^2}\left[\frac{1}{S_r}\left\{\left(E_r I_r + \bar{Z}E_r A_r C_1\left(\frac{h}{2}\right)^3\right)\left(\frac{\partial^2 w_I^1}{\partial\alpha_2^2}\right)\right.\right.$$
$$\left.\left. -\left(\bar{Z}E_r A_r + E_r A_r C_1\left(\frac{h}{2}\right)^3\right)\left(\frac{\partial v_I^1}{\partial\alpha_2}+\frac{W_I^1}{R}\right)\right)\right\}$$
$$-\frac{\partial^2}{\partial\alpha_1\partial\alpha_2}\left[\frac{1}{S_s}\left(G_s J_s\frac{\partial^2 w_I^1}{\partial\alpha_1\partial\alpha_2}\right)\right.$$
$$\left. +\frac{1}{S_r}\left(G_r J_r\frac{\partial^2 w_I^1}{\partial\alpha_1\partial\alpha_2}\right)\right] = 0 \quad (54)$$

$$-Q^1_{\alpha_1\alpha_3} - 3C_1 R^1_{\alpha_1\alpha_3} + M^1_{\alpha_1\alpha_1,\alpha_1} + M^1_{\alpha_1\alpha_2,\alpha_2}$$
$$- C_1(P^1_{\alpha_1\alpha_1,\alpha_1} + P^1_{\alpha_1\alpha_2,\alpha_2})$$
$$+\frac{\partial}{\partial\alpha_1}\left[\frac{1}{S_s}\left\{\left(\frac{h}{2}-C_1\left(\frac{h}{2}\right)^3\right)E_s A_s\left(\frac{\partial w_I^1}{\partial\alpha_1}\right)\right.\right. \quad (55)$$
$$\left.\left. -\bar{Z}_s A_s E_s\left(\frac{h}{2}-C_1\left(\frac{h}{2}\right)^3\right)\left(\frac{\partial^2 w_I^1}{\partial\alpha_1^2}\right)\right\}\right] = 0$$

$$-Q^1_{\alpha_1\alpha_3} + -3C_1 R^1_{\alpha_2\alpha_3} + M^1_{\alpha_2\alpha_1,\alpha_1} + M^1_{\alpha_2\alpha_2,\alpha_2}$$
$$- C_1(P^1_{\alpha_1\alpha_2,\alpha_1} + P^1_{\alpha_2\alpha_2,\alpha_2})$$
$$+\frac{\partial}{\partial\alpha_2}\left[\frac{1}{S_r}\left\{\left(\frac{h}{2}-C_1\left(\frac{h}{2}\right)^3\right)E_r A_r\left(\frac{\partial v_I^1}{\partial\alpha_2}+\frac{w_I^1}{R}\right)\right.\right. \quad (56)$$
$$\left.\left. -\bar{Z}_r E_r A_r\left(\frac{h}{2}-C_1\left(\frac{h}{2}\right)^3\right)\left(\frac{\partial^2 w_I^1}{\partial\alpha_2^2}\right)\right\}\right] = 0$$

where the superscript "1" denotes the state of stability. In aforementioned expressions, $N^0_{\alpha_1\alpha_1}$ and $N^0_{\alpha_2\alpha_2}$ represent the pre-buckling force resultants of the SP reinforced by agglomerated graded CNTs which deemed that there are no shear and axial forces along α_2-direction.

2.4 Solution methodology

The stability equations, Eqs. (52)-(56), is numerically solved to determine the critical buckling load of the CNTCR SP reinforced by agglomerated graded CNTs subjected to axial and lateral loads. It has been adopted that the forces N^0_{xx} and N^0_{yy} in x and y directions, respectively, with following assumption are obtained as follows

$$N^0_{xx} = -\frac{F}{R\Theta}, \qquad N^0_{yy} = -PR$$
$$\Upsilon = \frac{P}{R^2 F\Theta} \quad (57)$$

The two edges of the SP are assumed to be simply supported and, as a result, the boundary conditions are given by

$$v_0^1 = w_0^1 = M_{xx}^{\ 1} = N_{xx}^{\ 1} = \phi^1 = 0 \qquad \text{at} \quad x = 0, L \quad (58)$$

Assuming the simply supported boundary conditions at $\alpha_2 = 0$ and $\alpha_2 = \Theta$, the following approximate solution is proposed for the displacement fields as follows

$$u_1 = u_{0n}(\alpha_1)\sin\left(\frac{n\pi\alpha_2}{\Theta}\right)$$
$$v_1 = v_{0n}(\alpha_1)\cos\left(\frac{n\pi\alpha_2}{\Theta}\right)$$
$$w_1 = w_{0n}(\alpha_1)\sin\left(\frac{n\pi\alpha_2}{\Theta}\right) \quad (59)$$
$$\psi_1 = \psi_n(\alpha_1)\sin\left(\frac{n\pi\alpha_2}{\Theta}\right)$$
$$\phi_1 = \phi_n(\alpha_1)\cos\left(\frac{n\pi\alpha_2}{\Theta}\right)$$

where $n = 1, 2,...$ is the number of half waves in α_2-direction. At this step, the partial derivatives obtained by substituting Eq. (59) into the Eqs. (52)-(56) have to be specified in their discrete form by means of the GDQM. The interested reader can find the basic aspects and all explanations of GDQM in (Shu 2012, Sobhani Aragh *et al.* 2012). In compact vector notation, the discrete form of stability equations along with the associated boundary conditions can be conveniently written as

$$\begin{bmatrix} \left[A_{bb} \right] & \left[A_{bd} \right] \\ \left[A_{db} \right] & \left[A_{dd} \right] \end{bmatrix} \begin{Bmatrix} d_b \\ d_d \end{Bmatrix} + F \begin{bmatrix} 0 & 0 \\ \left[A_{g_1} \right] & \left[A_{g_2} \right] \end{bmatrix} \begin{Bmatrix} d_b \\ d_d \end{Bmatrix} = 0 \quad (60)$$

in which subscripts 'd' and 'b' denote domain and boundary, respectively. Then, through the condensation of boundary degrees of freedom, the critical buckling load of a SP reinforced by graded agglomerated CNTs is obtained from

$$\left(\left[A_{dd} \right] - \left[A_{dd} \right] \left[A_{bb} \right]^{-1} \left[A_{bd} \right] \right) \{ d_d \}$$
$$+ F \left(\left[A_{g_2} \right] - \left[A_{g_1} \right] \left[A_{bb} \right]^{-1} \left[A_{bd} \right] \right) = 0 \quad (61)$$

3. Results and discussion

3.1 Validation of the present work

Due to lack of relevant available literature regarding the mechanical buckling of the continuously graded CNTRC SP reinforced by ring and stringer stiffeners for direct comparison, validation of the presented methodology is carries out

in such a way that the results are compared to those of the isotropic and continuously graded CNTRC cylindrical shells. The critical buckling load of an isotropic stiffened and un-stiffened cylindrical shells made of alumina (Brush and Almroth 1975) is chosen for the first comparison case. The reference geometry for this compari-son case is a cylindrical shell with $L/R = 1$ and $R = 0.3$. As can be observed in Table 1, the results achieved from this comparison are in good agreement.

The accuracy of this work using the two-parameter EMT is compared with those of the ERM by Shen (2011) with graded aligned, straight CNTs, as tabulated in Table 2. In this table, Poly (methyl methacrylate), referred to as PMMA, is chosen for the matrix phase, and the (10, 10) SWCNTs are selected as reinforcements. In addition, the temperature is assumed to be $T = 300$ K (room temperature) at which there are no thermal strains. The un-stiffened cylindrical shell with $L = 160.9$ mm is subjected to an axial load. As can be seen in this comparison, there is well agreement between the results proving the accuracy of the present methodology. According to Table 2, it is worth noting that critical buckling load determined by EMT for the two types of CNTs profiles and Uniform profile are higher than those of the ERM.

3.2 Parametric studies

In this section, parametric studies for mechanical buckling of agglomerated CNTCR SP subjected to axial and lateral loads for various kinds of CNT volume fraction profiles and geometrical parameters are presneted. For the numerical results elaborated in this section, the buckling load intensity factor is stated in terms of a parameter $I_{cr} = F_{cr}L^2/\pi^2 D_c$ in which D_c is a rigidity modulus of the SP composed of ceramic material which equals $D_c = E_c h^3/12(1 - v_c^2)$. Note that the stiffeners are made by Alumina, the same as the matrix of the nanocomposite. The (10,10) SWCNTs as the reinforcement phase and Alumina as the ceramic matrix (Reddy and Chin 1998, Mo *et al.* 2005) are chosen. Han and Elliott (Mo *et al.* 2005) picked for $E_{CNT}^{11} = 600$ GPa, $E_{CNT}^{22} = 10$ GPa, $E_{CNT}^{12} = 17.2$ GPa for (10,10) SWCNTs. Such a low figure of the modulus of elasticity, as reported by (Odegard *et al.* 2003), is owing to the fact that the effective thickness of CNTs is presupposed to be 0.34 nm or more. Nevertheless, the effective thickness of SWCNTs should be smaller than 0.142 nm (Wang and Zhang 2008). Hence, the material properties and effective thickness of SWCNTs used for the present study suitably

Table 1 Comparison of the critical buckling load for various values of mid-radius to thickness ratio, R/h ($L/R = 1$, $R = 0.3$ m)

R/h	Un-stiffened		Stiffened	
	Present	Brush and Almroth 1975	Present	Brush and Almroth 1975
30	26. 4529	26.2390	26.5272	26.3023
50	9. 5116	9.4460	9.5533	9.4827
100	2. 3891	2.3615	2.4076	2.3659
200	0.5981	0.5904	0.6086	0.5988
300	0.2663	0.2623	0.2730	0.2672

Table 2 Comparisons of critical axial buckling load (kN) for un-stiffened continuously graded CNTRC CS with aligned and straight CNTs ($R/h = 100$, $h = 1$ mm, $\underline{z} = L^2/Rh$, $T = 300$ K)

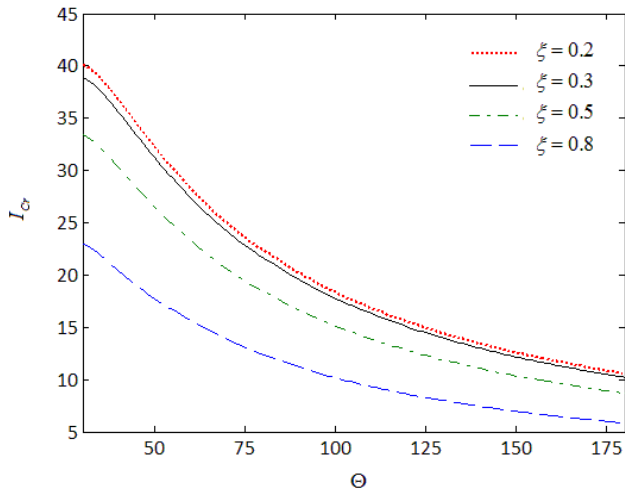|		$V_{CNT}^* = 0.12$		$V_{CNT}^* = 0.17$		$V_{CNT}^* = 0.28$	
		Uniform profile	Profile-X	Uniform profile	Profile-X	Uniform profile	Profile-X
$\underline{Z} = 100$	Shen 2011	18.75	21.81	30.43	35.53	37.77	47.18
	Present	19.82	22.93	31.57	36.45	39.01	48.80
$\underline{Z} = 300$	Shen 2011	19.35	22.06	31.11	37.06	39.60	46.52
	Present	20.00	23.33	32.09	38.13	40.55	48.87
$\underline{Z} = 500$	Shen 2011	18.72	21.37	30.57	35.14	37.31	45.99
	Present	19.91	22.14	32.11	36.46	38.29	46.80

Fig. 3 Effect of the agglomeration parameter, ξ, on the buckling load intensity factor of the SP with CNT distribution of the Profile-X ($L/R = 2$, $S = 20$, $N_r = N_s = 15$, $\mu = 0.1$)
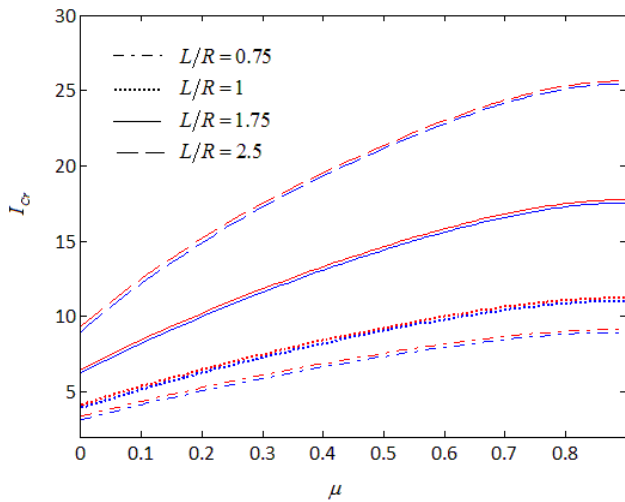

Fig. 4 Variation of buckling load intensity factor of the CNTRC SP with the agglomeration parameter, μ, and L/R ratio: Red line - exterior stiffeners; Blue line – interior stiffeners ($N_r = N_s = 15$, $\xi = 0.9$, $S = 20$, $\Theta = \pi/2$)

panel angle, the buckling load intensity factor declines. The decline rate of the intensity factor is significantly more sensible for the smaller values of panel angle ($\Theta < 100$). Further, the increase of the agglomeration parameter, ξ, declines the intensity factor with higher consequences on the SP with larger panel angle. This implies that increasing agglomeration parameter, ξ, has a deteriorating impact on the stability of the SP owing to raising the CNT agglomerations.

Fig. 4 demonstrates the variation of buckling load intensity factor of the continuously graded CNTRC SP with L/R ratio and the agglomeration parameter, μ. In this figure, it is assumed that the CNT distribution profile is assumed to be Profile-X. It can be inferred from this figure that the variation of the critical buckling load with the agglomeration parameter, μ, is far more drastic for the SPs with higher values of L/R ratio. On the contrary to the agglomeration
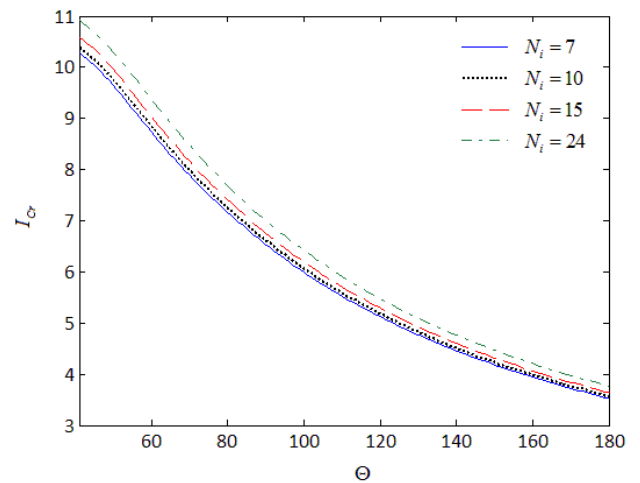

Fig. 5 Effect of the number of stiffeners on the buckling load intensity factor of the continuously graded CNTRC SP for different values of panel angle ($\mu = \xi = 0.7$, $S = 30$, $L/R = 1$)
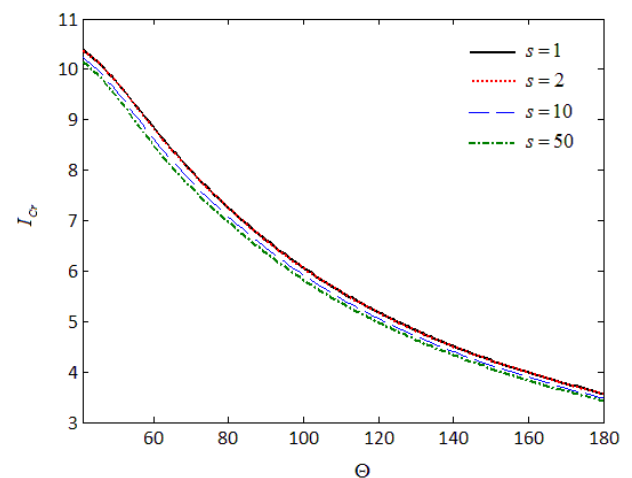

Fig. 6 Influences of sigmoidal parameter, s, and panel angle on the intensity factor of SP reinforced by agglomerated graded CNTs ($\mu = \xi = 0.7$, $S = 30$, $L/R = 1$, $N_r = N_s = 15$)

are selected based on the MD simulation results reported by Shen and Zhang (Shen and Zhang 2010). The material properties of the (10,10) SWCNTs are $E_{CNT}^{11} = 5.6466$ TPa, $E_{CNT}^{22} = 7.08$ TPa, $E_{CNT}^{12} = 1.9445$ TPa, and $v_{CNT}^{12} = 0.175$ at room temperature (300 K). It is worthwhile noting that the effective wall thickness for (10,10)-tube is 0.067 nm, which fulfills the Vodenitcharova-Zhang criterion (Wang and Zhang 2008), and the figure of 0.34 nm for tube wall thickness is an unsatisfactory assumption for SWCNTs. The CNT volume fraction used in this part is $V_{CNT}^{*} = 0.28$ unless the otherwise indicated.

The variation the buckling load intensity factor of the agglomerated CNTRC SP with panel angle, Θ, is presented in Fig. 3 for different values of the agglomeration parameter, ξ. As can be seen in this figure, by increasing the
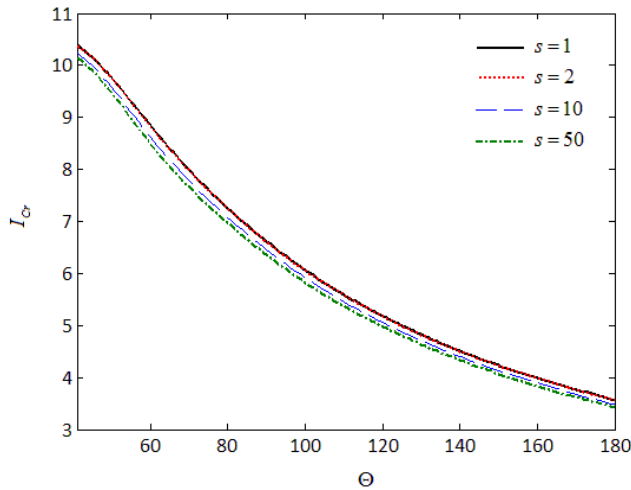
Fig. 7 Effect of various CNT profiles on the buckling load intensity factor of the SP reinforced by agglomerated graded CNTs ($\zeta = 1$, $S = 20$, $N_r = N_s = 20$, $s = 1$, $L/R = 2$)
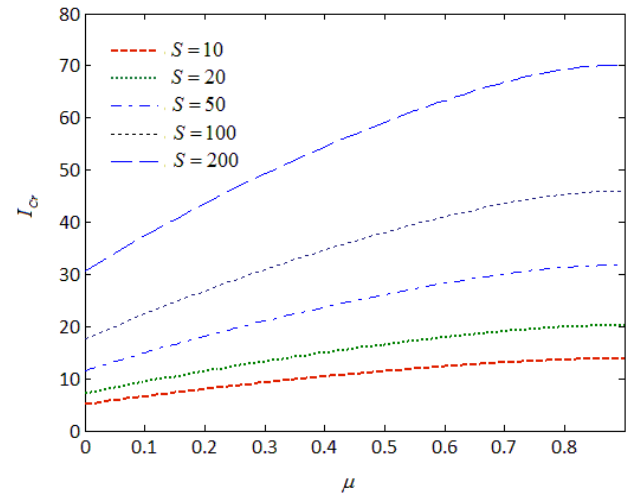

Fig. 8 Variation of buckling load intensity factor with the mid-radius to the thickness ratio, S, for different values of the agglomeration parameter, μ ($\xi = 0.9$, $\Theta = \pi/2$, $L/R = 2$, $N_r = N_s = 7$)

parameter, ξ, the increase of the agglomeration parameter, μ, increases the stability of the SP. In addition, it is worth noting that stiffening the panel with exterior stiffeners increases the buckling load intensity factor compared with exterior stiffeners.

The effect of the number of stiffeners on the buckling load intensity factor of the continuously graded CNTRC SP for different values of panel angle is studied in Fig. 5. According to this figure, the buckling load intensity factor rises by increasing the number of the stiffeners. Influences of sigmoidal parameter, s, and panel angle on the intensity factor of SP reinforced by agglomerated graded CNTs are investigated in Fig. 6. From Fig. 6, one can find the benefits of grading of CNTs through the thickness of the panel in increasing the critical mechanical buckling load compared to that of the discretely laminated composite. Increasing the sigmoidal parameter, s, the buckling response of the SP reaches to that of the two-lamina composite such that the CNT volume fractions of the outer and inner laminas are 17 percent and 0 percent, respectively. As can be seen from this figure, the impact of the smoothly gradation of the CNTs on the critical buckling load can be found more appreciable in the SP.

Fig. 6 presents the impacts of various CNT profiles on the buckling load intensity factor of the SP reinforced by agglomerated graded CNTs. According to the achieved results, the highest value of the critical buckling load can be obtained by using the Profile-X. This means that continuously distributing of CNTs adjacent to the inner and outer panel's surface results in improving the stiffness of the SP and, as a consequence, inclining the critical buckling load. It is worthwhile indicating that the effect of the CNTs distribution through the panel's thickness on the critical mechanical buckling load is remarkably more evident for the smaller values of panel angle. The variation of buckling load intensity factor with the mid-radius to the thickness ratio, S, for different values of the agglomeration parameter, μ, is depicted in Fig. 7. It is interesting to note that the effect of the agglomeration parameter, μ, on the critical buckling load is substantially more obvious for the thinner SP.

Table 3 Buckling load intensity factor of the SCS reinforced by agglomerated graded CNTs for various CNT profiles and the number of the ring and stringer stiffeners, N_i ($L/R = 1$, $\xi = 1$, $s = 1$)

S	N_i	Interior stiffeners					Exterior stiffeners				
		Profile-$\wedge$	Profile-X	Profile-O	Uniform profile	Sigmoidal profile	Profile-$\wedge$	Profile-X	Profile-O	Uniform profile	Sigmoidal profile
10	6	0.8903	0.9497	0.8457	0.9116	0.8286	0.8912	0.9506	0.8467	0.9125	0.8295
	15	0.8906	0.9498	0.8458	0.9119	0.8288	0.8926	0.9519	0.8480	0.9139	0.8308
	20	0.8907	0.9501	0.8459	0.9122	0.8289	0.8934	0.9527	0.8488	0.9146	0.8315
	24	0.8909	0.9503	0.8461	0.9125	0.8291	0.8941	0.9533	0.8494	0.9152	0.8321
50	6	1.6305	1.7428	1.5484	1.6687	1.5167	1.6416	1.7533	1.5589	1.6792	1.5269
	15	1.6308	1.7431	1.5486	1.6690	1.5171	1.6583	1.7693	1.5749	1.6952	1.5424
	20	1.6309	1.7433	1.5488	1.6692	1.5173	1.6676	1.7782	1.5838	1.7041	1.5510
	24	1.631	1.7434	1.5489	1.6693	1.5174	1.6750	1.7853	1.5909	1.7112	1.5578

4. Conclusions

The present paper studied the mechanical buckling response of the continuously graded CNTRC SP agglomerated by CNTs subjected to axial and lateral loads. Notwithstanding most available studies in which the stiffener effects were smeared out over the respective stiffener spacing, in this study, the stiffeners have been modeled as Euler-Bernoulli beams. A two-parameter EMT model was employed to derive the effective material moduli of the CNTRC. The stability equations derived by means of the adjacent equilibrium criterion were solved via the GDQM in combination with the trigonometric expansion. According to the numerical results obtained, the following conclusions can be made:

- By increasing the panel angle, the buckling load intensity factor declines. Note that the decline rate of the intensity factor is significantly more sensible for the smaller values of panel angle.
- The results reveal that increasing agglomeration parameter, ζ, has a deteriorating impact on the stability of the SP owing to raising the CNT agglomerations.
- Stiffening the panel with exterior stiffeners increases the buckling load intensity factor compared with exterior stiffeners.
- Continuously distributing of CNTs adjacent to the inner and outer panel's surface results in improving the stiffness of the SP and, as a consequence, inclining the critical buckling load.
- It has been inferred that the impact of the agglomeration parameter, μ, on the critical buckling load is substantially more obvious for the thinner SP.

References

Bich, D.H., Van Dung, D., Nam, V.H. and Phuong, N.T. (2013), "Nonlinear static and dynamic buckling analysis of imperfect eccentrically stiffened functionally graded circular cylindrical thin shells under axial compression", *Int. J. Mech. Sci.*, **74**, 190-200.

Bououdina, M. (Editor) (2014), *Handbook of Research on Nanoscience, Nanotechnology, and Advanced Materials*, IGI Global.

Brush, D.O. and Almroth, B.O. (1975), *Buckling of Bars, Plates, and Shells*, McGraw-Hill Book Co., New York, NY, USA, 394 p.

Cristescu, N.D., Craciun, E.M. and Soós, E. (2003), *Mechanics of Elastic Composites*, CRC Press.

Duc, N.D. and Thang, P.T. (2014), "Nonlinear buckling of imperfect eccentrically stiffened metal–ceramic–metal S-FGM thin circular cylindrical shells with temperature-dependent properties in thermal environments", *Int. J. Mech. Sci.*, **81**, 17-25.

Dung, V.D. and Chan, D.Q. (2017), "Analytical investigation on mechanical buckling of FGM truncated conical shells reinforced by orthogonal stiffeners based on FSDT", *Compos. Struct.*, **159**, 827-841.

Dung, V.D. and Hoa, K.L. (2013), "Research on nonlinear torsional buckling and post-buckling of eccentrically stiffened functionally graded thin circular cylindrical shells", *Compos. Part B: Eng.*, **51**, 300-309.

Eshelby, J.D. (1957), "The determination of the elastic field of an ellipsoidal inclusion, and related problems", *Proceedings of the Royal Society of London A: Mathematical, Physical and Engineering Sciences*, The Royal Society of London, August, Vol. 241, No. 1226, pp. 376-396.

Fantuzzi, N., Tornabene, F., Bacciocchi, M. and Dimitri, R. (2016), "Free vibration analysis of arbitrarily shaped functionally graded carbon nanotube-reinforced plates", *Compos. Part B: Eng.*, **115**, 384-408.

Fidelus, J.D., Wiesel, E., Gojny, F.H., Schulte, K. and Wagner, H.D. (2005), "Thermo-mechanical properties of randomly oriented carbon/epoxy nano-composites", *Compos. Part A: Appl. Sci. Manuf.*, **36**(11), 1555-1561.

Formica, G. and Lacarbonara, W. (2017), "Three-dimensional modeling of interfacial stick-slip in carbon nanotube nano-composites", *Int. J. Plastic.*, **88**, 204-217.

Formica, G., Lacarbonara, W. and Alessi, R. (2010), "Vibrations of carbon nanotube-reinforced composites", *J. Sound Vib.*, **329**(10), 1875-1889.

García-Macías, E., Rodriguez-Tembleque, L., Castro-Triguero, R. and Sáez, A. (2017), "Buckling analysis of functionally graded carbon nanotube-reinforced curved panels under axial compression and shear", *Compos. Part B: Eng.*, **108**, 243-256.

Gkikas, G., Barkoula, N.M. and Paipetis, A.S. (2012), "Effect of dispersion conditions on the thermo-mechanical and toughness properties of multi walled carbon nanotubes-reinforced epoxy", *Compos. Part B: Eng.*, **43**(6), 2697-2705.

Han, Y. and Elliott, J. (2007), "Molecular dynamics simulations of the elastic properties of polymer/carbon nanotube composites", *Computat. Mater. Sci.*, **39**(2), 315-323.

Hedayati, H. and Sobhani Aragh, B. (2012), "Influence of graded agglomerated CNTs on vibration of CNT-reinforced annular sectorial plates resting on Pasternak foundation", *Appl. Math. Computat.*, **218**(17), 8715-8735.

Iijima, S. (1991), "Helical microtubules of graphitic carbon", *Nature*, **354**(6348), 56-58.

Kamarian, S., Salim, M., Dimitri, R. and Tornabene, F. (2016), "Free vibration analysis of conical shells reinforced with agglomerated carbon nanotubes", *Int. J. Mech. Sci.*, **108**, 157-165.

Lei, Z.X., Liew, K.M. and Yu, J.L. (2013), "Buckling analysis of functionally graded carbon nanotube-reinforced composite plates using the element-free kp-Ritz method", *Compos. Struct.*, **98**, 160-168.

Lim, C.W., Ma, Y.F., Kitipornchai, S., Wang, C.M. and Yuen, R.K. (2003), "Buckling of vertical cylindrical shells under combined end pressure and body force", *J. Eng. Mech.*, **129**(8), 876-884.

Low, I.M. (Editor) (2014), *Advances in Ceramic Matrix Composites*, Woodhead Publishing.

Madani, H., Hosseini, H. and Shokravi, M. (2016), "Differential cubature method for vibration analysis of embedded FG-CNT-reinforced piezoelectric cylindrical shells subjected to uniform and non-uniform temperature distributions", *Steel Compos. Struct., Int. J.*, **22**(4), 889-913.

Meguid, S.A. and Sun, Y. (2004), "On the tensile and shear strength of nano-reinforced composite interfaces", *Mater. Des.*, **25**(4), 289-296.

Mehrabadi, S.J. and Sobhani Aragh, B. (2014), "Stress analysis of functionally graded open cylindrical shell reinforced by agglomerated carbon nanotubes", *Thin-Wall. Struct.*, **80**, 130-141.

Mo, C.B., Cha, S.I., Kim, K.T., Lee, K.H. and Hong, S.H. (2005), "Fabrication of carbon nanotube reinforced alumina matrix nano-composite by sol-gel process", *Mater. Sci. Eng.: A*, **395**(1), 124-128.

Moradi-Dastjerdi, R. (2016), "Wave propagation in functionally graded composite cylinders reinforced by aggregated carbon nanotube", *Struct. Eng. Mech., Int. J.*, **57**(3), 441-456.

Moradi-Dastjerdi, R. and Momeni-Khabisi, H. (2016), "Dynamic analysis of functionally graded nanocomposite plates reinforced by wavy carbon nanotube", *Steel Compos. Struct., Int. J.*, **22**(2), 277-299.

Mori, T. and Tanaka, K. (1973), "Average stress in matrix and average elastic energy of materials with misfitting inclusions", *Acta Metal.*, **21**(5), 571-574.

Najafizadeh, M.M., Hasani, A. and Khazaeinejad, P. (2009), "Mechanical stability of functionally graded stiffened cylindrical shells", *Appl. Math. Model.*, **33**(2), 1151-1157.

Nguyen, H.X., Nguyen, T.N., Abdel-Wahab, M., Bordas, S.P., Nguyen-Xuan, H. and Vo, T.P. (2017), "A refined quasi-3D isogeometric analysis for functionally graded microplates based on the modified couple stress theory", *Comput. Method. Appl. Mech. Eng.*, **313**, 904-940.

Odegard, G.M., Gates, T.S., Wise, K.E., Park, C. and Siochi, E.J. (2003), "Constitutive modeling of nanotube–reinforced polymer composites", *Compos. Sci. Technol.*, **63**(11), 1671-1687.

Phung-Van, P., Abdel-Wahab, M., Liew, K.M., Bordas, S.P. and Nguyen-Xuan, H. (2015), "Isogeometric analysis of functionally graded carbon nanotube-reinforced composite plates using higher-order shear deformation theory", *Compos. Struct.*, **123**, 137-149.

Phung-Van, P., Ferreira, A.J., Nguyen-Xuan, H. and Wahab, M.A. (2017a), "An isogeometric approach for size-dependent geometrically nonlinear transient analysis of functionally graded nanoplates", *Compos. Part B: Eng.*, **118**, 125-134.

Phung-Van, P., Lieu, Q.X., Nguyen-Xuan, H. and Wahab, M.A. (2017b), "Size-dependent isogeometric analysis of functionally graded carbon nanotube-reinforced composite nanoplates", *Compos. Struct.*, **166**, 120-135.

Reddy, J.N. (1984), "A refined nonlinear theory of plates with transverse shear deformation", *Int. J. Solids Struct.*, **20**(9), 881-896.

Reddy, J.N. (2004), *Mechanics of Laminated Composite Plates and Shells*: *Theory and Analysis*, CRC Press.

Reddy, J.N. and Chin, C.D. (1998), "Thermo-mechanical analysis of functionally graded cylinders and plates", *J. Therm. Stress.*, **21**(6), 593-626.

Selim, B.A., Zhang, L.W. and Liew, K.M. (2015), "Vibration analysis of CNT reinforced functionally graded composite plates in a thermal environment based on Reddy's higher-order shear deformation theory", *Compos. Struct.*, **156**, 276-290.

Shen, H.S. (2009), "Nonlinear bending of functionally graded carbon nanotube-reinforced composite plates in thermal environments", *Compos. Struct.*, **91**(1), 9-19.

Shen, H.S. (2011), "Postbuckling of nanotube-reinforced composite cylindrical shells in thermal environments, Part I: Axially-loaded shells", *Compos. Struct.*, **93**(8), 2096-2108.

Shen, H.S. (2012), "Thermal buckling and postbuckling behavior of functionally graded carbon nanotube-reinforced composite cylindrical shells", *Compos. Part B: Eng.*, **43**(3), 1030-1038.

Shen, H.S. (2016), *Functionally Graded Materials*: *Nonlinear Analysis of Plates and Shells*, CRC Press.

Shen, H.S. and Zhang, C.L. (2010), "Thermal buckling and postbuckling behavior of functionally graded carbon nanotube-reinforced composite plates", *Mater. Des.*, **31**(7), 3403-3411.

Shi, D.L., Feng, X.Q., Huang, Y.Y., Hwang, K.C. and Gao, H. (2004), "The effect of nanotube waviness and agglomeration on the elastic property of carbon nanotube-reinforced composites", *J. Eng. Mater. Technol.*, **126**(3), 250-257.

Shu, C. (2012), *Differential Quadrature and its Application in Engineering*, Springer Science & Business Media.

Sobhaniaragh, B. (2014), "Vibration and thermal stress analyses of functionally graded materials", Ph.D. Dissertation; Ghent University, Belgium.

Sobhani Aragh, B., Barati, A.N. and Hedayati, H. (2012), "Eshelby–Mori–Tanaka approach for vibrational behavior of continuously graded carbon nanotube-reinforced cylindrical panels", *Compos. Part B: Eng.*, **43**(4), 1943-1954.

Sobhani Aragh, B., Farahani, E.B. and Barati, A.N. (2013), "Natural frequency analysis of continuously graded carbon nanotube-reinforced cylindrical shells based on third-order shear deformation theory", *Math. Mech. Solids*, **18**(3), 264-284.

Talò, M., Krause, B., Pionteck, J., Lanzara, G. and Lacarbonara, W. (2016), "An updated micromechanical model based on morphological characterization of carbon nanotube nano-composites", *Compos. Part B: Eng.*, **115**, 70-78.

Tornabene, F., Fantuzzi, N., Bacciocchi, M. and Viola, E. (2016), "Effect of agglomeration on the natural frequencies of functionally graded carbon nanotube-reinforced laminated composite doubly-curved shells", *Compos. Part B: Eng.*, **89**, 187-218.

Tran, L.V., Phung-Van, P., Lee, J., Wahab, M.A. and Nguyen-Xuan, H. (2016), "Isogeometric analysis for nonlinear thermomechanical stability of functionally graded plates", *Compos. Struct.*, **140**, 655-667.

Wang, C.Y. and Zhang, L.C. (2008), "A critical assessment of the elastic properties and effective wall thickness of single-walled carbon nanotubes", *Nanotechnology*, **19**(7), 075705.

Wang, M., Li, Z.M. and Qiao, P. (2016), "Semi-analytical solutions to buckling and free vibration analysis of carbon nanotube-reinforced composite thin plates", *Compos. Struct.*, **144**, 33-43.

Zhang, L.W., Lei, Z.X. and Liew, K.M. (2015), "An element-free IMLS-Ritz framework for buckling analysis of FG–CNT reinforced composite thick plates resting on Winkler foundations", *Eng. Anal. Boundary Elem.*, **58**, 7-17.

Zhu, P., Lei, Z.X. and Liew, K.M. (2012), "Static and free vibration analyses of carbon nanotube-reinforced composite plates using finite element method with first order shear deformation plate theory", *Compos. Struct.*, **94**(4), 1450-1460.

CC